Journal of Thermal Analysis and Calorimetry (2022) 147:4983–4993
https://doi.org/10.1007/s10973-021-10900-5

Experimental study of electric furnace ferronickel slag as a supplementary cementitious material in massive high-strength concrete

Yuqi Zhou[1] · **Chunfang Shi**[1]

Received: 29 August 2020 / Accepted: 10 May 2021 / Published online: 20 June 2021

Abstract
This study aims to investigate the feasibility of using electric furnace ferronickel slag (EFFS) as a supplementary cementitious material (SCM) in massive high-strength concrete (MHC). The workability, hydration heat, and pore structure of fresh and hardened paste are characterized using a rotor rheometer, an isothermal calorimeter, thermogravimetric analysis, and mercury intrusion porosimetry. The adiabatic temperature rise, autogenous shrinkage, mechanical properties, and chloride permeability of the concrete are investigated to examine the effect of EFFS. The results show that the utilization of EFFS as an SCM can improve the workability and reduce the hydration heat. The pore structure can be refined with the decrease in the w/b ratio. The addition of EFFS can reduce the adiabatic temperature rise and long-term autogenous shrinkage of concrete. Moreover, the incorporation of EFFS in concrete can improve the long-term strength and durability properties. These results support the advantages of EFFS, which can endow MHC with sufficient properties to resist thermal cracking and autogenous shrinkage cracking. The utilization of EFFS as an SCM will be a good step toward sustainable infrastructure development.

Keywords Electric furnace ferronickel slag · Massive high-strength concrete · Hydration heat · Adiabatic temperature rise · Autogenous shrinkage

Introduction

With the growth of infrastructure construction, particularly in developing countries, the demand for massive high-strength concrete (MHC) has increased drastically. This construction material is widely used in many engineering structures, such as high-rise building columns, bridge substructure members, and underground structures, especially the walls of subway tunnels [1, 2]. However, some challenges faced in the application of MHC include volumetric change due to autogenous shrinkage and cracking due to temperature stress [3]. Volumetric stability is a key factor that affects the durability and service life of concrete structures because most of the deformation is irreversible. The initial volumetric change of concrete is attributed to autogenous shrinkage in the first few weeks after pouring [4]. Autogenous shrinkage refers to the overall volume deformation of concrete without moisture changes or external forces during the hydration process under stable temperature conditions [5], due to which the internal volume will be reduced by 7–10% of the initial volume [3]. It is mainly related to the hydration kinetics, elastic modulus, viscosity, and stress relaxation of materials at an early age. In general, the higher the water–binder ratio, the lower the early autogenous shrinkage [6, 7], and the autogenous shrinkage of concrete with high water–binder ratios is minimal to negligible. Thus, the autogenous shrinkage of MHC is relatively large due to a low water–binder ratio and an abundant amount of binder. Additionally, moisturizing curing has no significant effect on MHC due to its relatively large volume.

Regarding the second challenge faced in the application of MHC, it is well acknowledged that the total heat in the concrete originates from the hydration of cementitious materials, including cement and mineral admixtures. The hydration heat of MHC increases the internal temperature. When internal heat is lost to the external atmosphere, there is a temperature difference between the cold exterior and the hot interior, which causes differences in free thermal dilation

✉ Yuqi Zhou
zhouyuqidoc@163.com

[1] China Construction First Group Construction and Development Co., Led.,, Beijing 100102, China

[8]. If the tensile stress due to free thermal dilation exceeds the tensile deformation capacity of the concrete, cracks will appear inside and on the surface of the concrete [8]. Compared to normal concrete, the fineness and content of cementitious materials in MHC are both increased, which leads to a higher hydration heat and a higher internal temperature. The registered maximum temperature in MHC is + 80 °C, while the ambient temperature is approximately + 15 °C [2, 9]. Consequently, thermal cracking during the cooling process is common in MHC.

To ensure the quality of concrete, the early age autogenous shrinkage and cracking sensitivity of MHC should be limited. Supplementary cementitious materials (SCMs) have been widely used for many years to achieve the high performance of MHC. The use of fly ash as an SCM to replace cement in MHC is a common and efficient method due to its low early activity [1, 10]. However, the reserves of fly ash are limited, and it is more expensive in some areas due to significant regional differences. Thus, other industrial residues must be explored to ensure the sustainability of MHC. Electric furnace ferronickel slag (EFFS) is an industrial waste produced during nickel smelting via the use of laterite, garnierite, or pentlandite ores at temperatures of about 1500–1600 °C [11, 12]. Depending on its sources and processing and cooling methods, EFFS generally consists of 30–54.5% SiO_2, 6.4–43.8% Fe_2O_3, 2.7–26.9% MgO, 1.5–12% CaO, and 2.5–8.3% $A1_2O_3$ [13–15]. Crystalline mineral phases in EFFS include olivine, enstatite, forsterite, diopside, and periclase [15, 16]. Regarding its physical properties, EFFS is generally characterized by low water absorption, high density, and high hardness [17, 18]. It is estimated that approximately 12–14 tons of EFFS are produced per 1 ton of nickel alloy [19, 20]. However, most EFFS is disposed of in an open environment, and it is not widely used as a potential SCM in cementitious systems. The major reasons for this are its decreased late-age volumetric stability due to its high periclase content, as well as environmental pollution resulting from the leaching of hazardous metals (Ni, Cr, Mn, and Co) as impacted by rain [21–23]. A slight amount of magnesium in EFFS may exist in the form of periclase [24]. The Mg^{2+} originating from periclase will react with OH^- to form brucite ($Mg(OH)_2$) during later ages, thereby increasing the risk of volumetric expansion [25]. Furthermore, the leaching of heavy metals has been proven to be harmful to both ground and underground water [26, 27]. However, with the continuous improvement of the smelting process, the contents of periclase and heavy metals in EFFS will become increasingly reduced. To prevent the rapid depletion of cement, the use of EFFS as a potential SCM, which is also an effective way to recycle EFFS resources, requires further investigation.

Some studies have proven that it is feasible to partially replace cement with EFFS. Rahman et al. [28] demonstrated that the use of a content of up to 50% of EFFS as an SCM had no significant effect on the water demand and setting times. They also found that the high content of magnesium present in EFFS in the form of stable forsterite ferroan did not take part in hydration leading to increased expansion [28]. Huang et al. [29] found that, although EFFS exhibited low activity under non-alkaline conditions and a coarsened pore structure that resulted in a reduction in compressive strength, it improved the resistance of the concrete to chloride ion penetration. Kim et al. [30] used three types of EFFS with different levels of fineness to replace cement and evaluated the effects on the properties of the concrete. They found that the addition of EFFS had negative effects on the early strength and carbonation resistance of the concrete, but it improved the chemical resistance to chloride and sulfate [30]. Moreover, the addition of EFFS with similar fineness to that of cement was found to notably reduce the adiabatic temperature and drying shrinkage, whereas finer EFFS did not produce the desired effect [30]. Both Saha et al. [31] and Li et al. [14] reported that the incorporation of EFFS could improve sulfate resistance, as the EFFS specimens exhibited low expansion and only a marginal loss in strength without visible surface cracking. Li et al. [14] also reported that, even under early steaming-curing conditions, the influences of the $(Mg, Fe)_2SiO_4$ and $MgSiO_3$ present in EFFS on the hydration products were very limited. Some researchers have also made efforts to prepare alkali-activated materials with proper performance via the incorporation of EFFS. Tao et al. [32–34] investigated the feasibility of using EFFS in alkali-activated fly ash-based materials manufacturing. They identified that the Si/Al ratio of the N–M–A–S gel increased due to the high silica content of EFFS, and the addition of 20% EFFS was found to achieve the maximal compressive strength with a finer pore structure and lower linear drying shrinkage [32–34]. Moreover, the addition of EFFS improved the fire resistance of alkali-activated fly ash-based materials [34]. Cao et al. [35] also investigated the feasibility of using EFFS in alkali-activated ground granulated blast-furnace slag (GGBS)-based materials and demonstrated that a low content (< 20%) of EFFS did not influence the properties of these materials. The incorporation of EFFS could increase the autogenous and drying shrinkages of water glass-activated GGBS materials, but could reduce the shrinkages of NaOH-activated GGBS materials.

From the preceding literature review, it is evident that the application of EFFS as a raw material in cement-based and alkali-activated material systems is feasible. However, the substitution rate of EFFS must be limited due to its low hydration activity. The existing research also reveals the potential of EFFS as a valuable source material for the manufacturing of MHC. However, so far, few studies have evaluated the influences of EFFS on the properties of MHC. The objective of the present study, therefore, is to develop

Table 1 Chemical compositions of OPC and EFFS (%)

Sample	SiO_2	Al_2O_3	Fe_2O_3	CaO	MgO	SO_3	NiO
OPC	21.10	6.33	4.22	54.86	2.6	2.66	–
EFFS	45.26	5.43	18.91	1.41	25.58	0.09	0.12

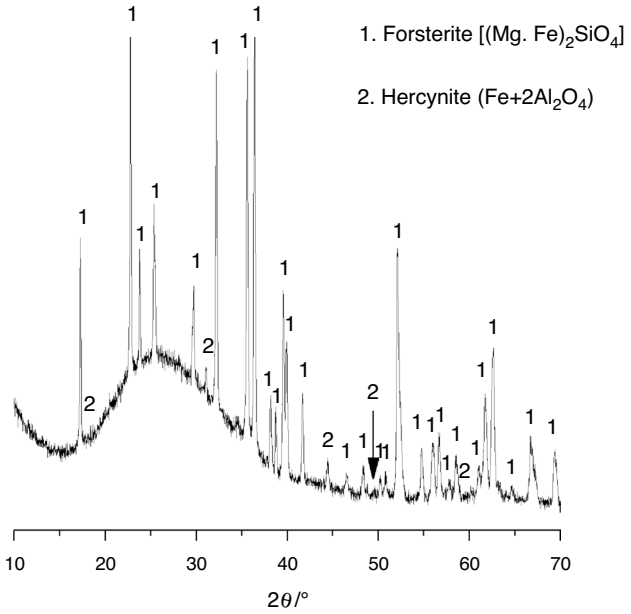

Fig. 1 XRD pattern of the EFFS

the feasible use of high-volume EFFS in MHC structures. The feasibility of simultaneously reducing the autogenous shrinkage and hydration temperature rise is subsequently explored.

Raw materials and test methods

Raw materials

The chemical compositions of ordinary Portland cement (OPC) and EFFS used in this study were determined by X-ray fluorescence (XRF) spectroscopy and are presented in Table 1. The EFFS was found to contain 25.58% MgO, and the high content of MgO in EFFS raises the concern of the long-term stability of concrete. Some studies [11, 28, 36] have investigated the soundness properties of concrete incorporated with EFFS. The soundness test results indicated that the EFFS samples did not exhibit any significant expansion because the MgO present in EFFS was chemically inert and stable. As shown in Fig. 1, the mineral phases of EFFS were tested by an X-ray diffractometer (XRD), and the presence of MgO was found to be in the form of forsterite. Two types of EEFS with different fineness were used in the experiments, the specific surface areas of which were 420 m^2kg^{-1} (EFFSA) and 550 m^2kg^{-1} (EFFSB), respectively.

Crushed limestone (5–25 mm) and natural river sand (fineness of 2.6) were used as coarse and fine aggregates, respectively. A polycarboxylate superplasticizer (PCE) was used to adjust the fluidity of the mixtures.

Table 2 Mix proportions of pastes

Samples	Cement /by mass %	EFFSA /by mass %	EFFSB /by mass %	Water-to-binder ratio
C	100			0.35
EFFSA-15	85	15		0.35
EFFSA-30	70	30		0.35
EFFSA-45	55	45		0.35
EFFSB-15	85		15	0.35
EFFSB-30	70		30	0.35
EFFSB-45	55		45	0.35

Preparation of paste specimens

The mix proportions of the pastes are reported in Table 2. Seven mix proportions of pastes were prepared with a water-binder (w/b) ratio of 0.35. The control paste specimen contained only cement (C). Portland cement was replaced by EFFSA and EFFSB at proportions of 15%, 30%, and 40% to produce the composite paste specimens.

Preparation of concrete and paste specimens

The mix proportions of the concretes are reported in Table 3. OPC was replaced by EFFSA and EFFSB at proportions of 30% and 40% with different w/b ratios to ensure that each group of concrete samples reached the same compressive strength level at an age of 28 d. Table 4 details the five groups of paste specimens according to the w/b ratios of the concrete specimens listed in Table 3.

Test methods

The rheological properties of the C, EFFSA-30, and EFFSB-30 pastes were evaluated with a rotor rheometer (RST, rotor: VT-40-20, S/N: 36 00,127, Brookfield, USA).

The exothermic rate and cumulative hydration heat of the pastes listed in Table 2 were measured at 25 and 50 °C using an isothermal calorimeter within 3 days.

Table 3 Mix proportions of concretes (kg/m^3)

Samples	C	EFFSA	EFFSB	Water	Fine aggregates	Coarse aggregates
C-0.35	460			161	750	1079
A30-0.29	322	138		133	768	1104
A40-0.26	276	184		120	775	1115
B30-0.31	322		138	143	764	1098
B40-0.28	276		184	129	772	1109

Table 4 Mix proportions of pastes

Samples	Cement (by mass %)	EFFSA (by mass %)	EFFSB (by mass %)	Water-to-binder ratio
C-0.35	100			0.35
A30-0.29	70	30		0.29
A40-0.26	60	40		0.26
B30-0.31	70		30	0.31
B40-0.28	60		40	0.28

Five groups of concrete specimens, namely C-0.35, A30-0.29, A40-0.26, B30-0.31, and B40-0.28, were prepared for the investigation of the adiabatic temperature rise. Each test was conducted on a 60-L specimen with an electrical thermometer embedded in its center. The concrete temperature rise was recorded every 10 min to obtain the curves of the adiabatic temperature rise.

The fresh concrete specimens C-0.35, A30-0.29, and A40-0.26 were cast in molds ($100 \times 100 \times 515$ mm), sealed with plastic, and placed between two support heads for the autogenous shrinkage test. Moreover, a plastic sheet was embedded in the mold to reduce the friction between the concrete and the mold. The entire setup was then placed indoors at a temperature of 20 °C and an RH of 60% for 7 d.

The five paste samples listed in Table 4 were prepared and cured in a curing box with a temperature adjusted according to the adiabatic temperature rise curve of concrete for the first 7 d, and were then cured in a standard curing room to 28 d. The hardened pastes were extracted at multiple testing ages for mercury intrusion porosimetry (MIP) testing and thermogravimetric (TG) analysis.

The compressive strengths of the C-0.35, A30-0.29, A40-0.26, B30-0.31, and B40-0.28 concrete specimens cured at temperature-match curing (TMC) conditions for 3, 28, and 90 d were tested. The splitting tensile strengths and chloride ion permeability of the five groups of concrete were tested at 28 and 90 d.

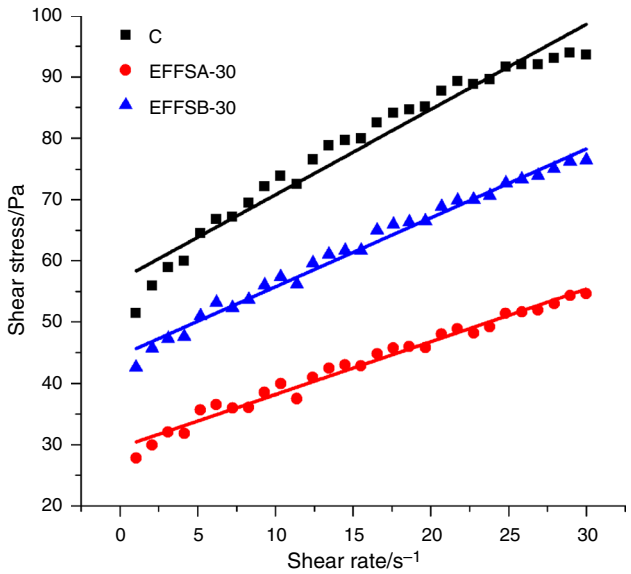

Fig. 2 The relationship between the shear rate and shear stress 3.2 Hydration heat

Results and discussion

Rheological performance

The rheological performance of the plain cement paste and the pastes containing 30% EFFSA and EFFSB were tested according to the rheological test program. First, the shear rate was increased from 0 to 10 rs^{-1} in 30 s, then decreased to 0 rs^{-1} in 30 s, followed by a 10 s static stop. The shear rate was then increased from 0 to 30 rs^{-1} in 60 s and decreased to 0 rs^{-1} in 60 s. Figure 2 presents the relationship between the shear rate and the shear stress, and the decreasing stage of the shear rate (from 30 s to 0 rs^{-1} in 60 s). The curves in Fig. 2 form a straight line via the Bingham model, as given by the following equation:

$$\tau = \tau_0 + \eta \cdot \gamma,$$

via which the yield stress (τ_0) and plastic viscosity (η_p) of the fresh pastes were calculated, where τ is the shear stress (Pa) and γ is the shear rate (s^{-1}).

It is evident that the pastes mixed with 30% EFFSA and EFFSB had lower yield stress and plastic viscosity as compared with pure cement group (C). The results indicate that the workability of the fresh pastes containing EFFS was improved, which was primarily due to the morphological effect of the glass beads and fine particles in the EFFS powder, which reduced the friction between the particles in the composite binder [26, 37]. However, with the increase in the specific surface area of EFFS from 420 m^2kg^{-1} (A) to 550 m^2kg^{-1} (B), the yield stress and plastic viscosity increased. This is because the particle size of EFFSB was smaller than that of EFFSA; at the same content, the number of direct particle-to-particle contacts was increased, and it was more difficult for solid particles to slide past one another [38]. Therefore, increasing the fineness of EFFS will decrease the workability of EFFS-cement paste.

Figures 3 and 4 show the exothermic rate and cumulative hydration heat curves for the hydration of cementitious materials in the pastes (listed in Table 2) within 3 d at 25 and 50 °C, respectively. The exothermic rate curves reveal that, at the normal curing temperature, the mixtures containing EFFS had lower heat evolution peaks than the control sample due to the decrease in the cement content of the composite pastes, which reduced the high-activity components. A comparison of the second exothermic peaks of the EFFSA and EFFSB samples at the same content indicates that the finer particles resulted in a higher exothermic peak. This implies that the increase in the fineness of EFFS can accelerate the hydration of the cement paste, as the finer particles may act as centers of nucleation and rapidly react with calcium hydroxide (CH), thereby accelerating the cement hydration. As shown in Fig. 3b, the cumulative hydration heat of the binders notably decreased with the increase in the EFFS content. This is because EFFS has very low contents of active components, such as CaO and Al_2O_3 [35] (as shown in Table 1). Therefore, the samples containing more EFFS tended to exhibit less early activity and lower hydration heat.

Figure 4a presents the exothermic rate of the binders at a high curing temperature of 50 °C. As expected, all binder reactivities were promoted by the high temperature, the heat evolution peaks occurred earlier (about 4 h), and the positions were higher. At the normal curing temperature, the heat evolution peaks of all binders were almost identical at 12 h. However, the heat evolution peak positions of the EFFS specimens were shifted due to the high curing temperature. It should be noted that the heat evolution peaks of the samples containing EFFSB were slightly shifted to left as compared to those of the plain cement sample. This may have been due to the stimulation of the reactivity of

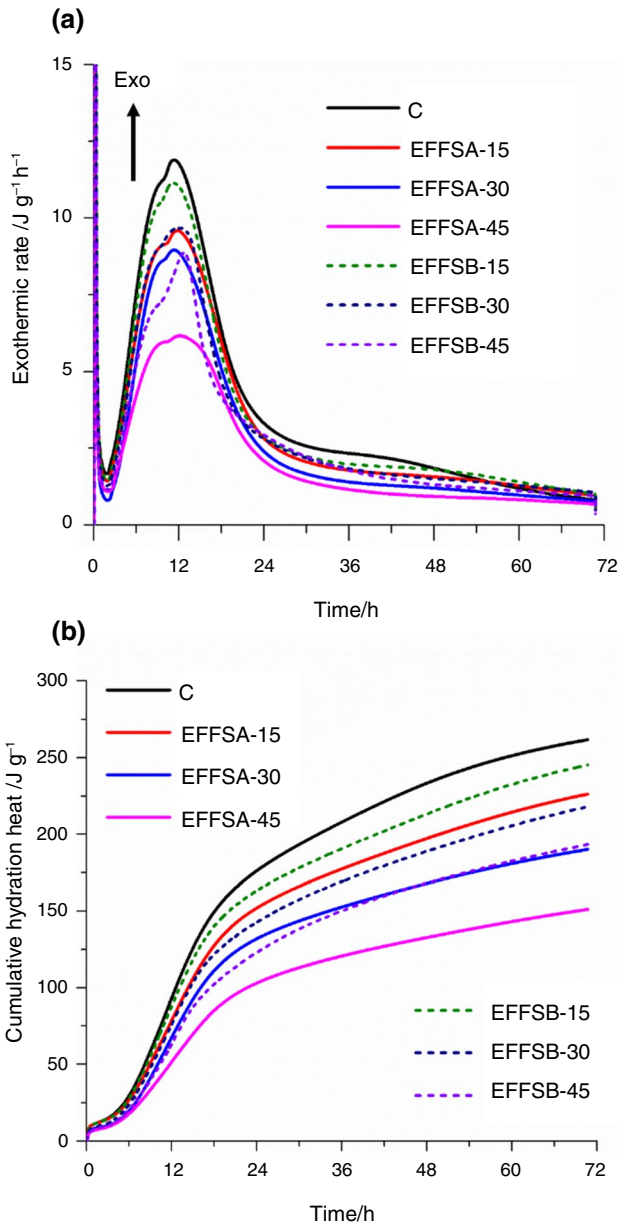

Fig. 3 **a** The exothermic rate and **b** the cumulative hydration heat of the pastes at 25 °C

EFFSB by the high temperature and the finer particles acting as nucleation centers, thereby accelerating cement hydration. As shown in Fig. 4b, the cumulative hydration heat of the binders at 50 °C presented a trend similar to that at 25 °C.

Adiabatic temperature rise of concrete

The curves of the adiabatic temperature rise of the concrete specimens are shown in Fig. 5, and details for each concrete mixture are summarized in Table 5. All concrete specimens with different w/b ratios had the same 28-day compressive strength level. For plain cement concrete with a w/b ratio of

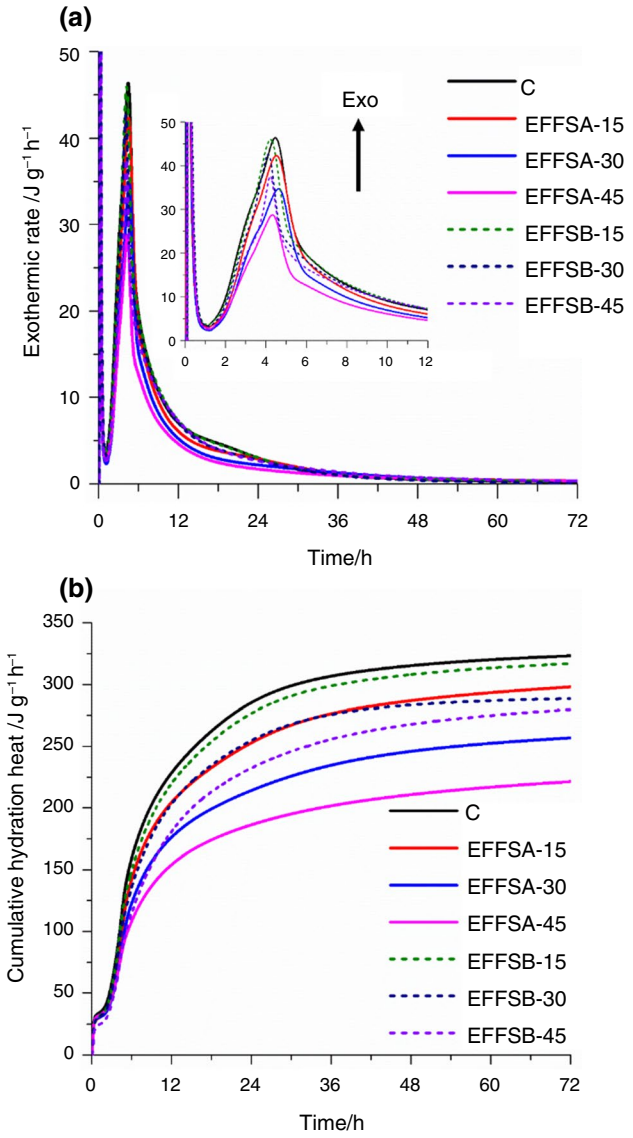

Fig. 4 **a** The exothermic rate and **b** the cumulative hydration heat of the pastes at 50 °C

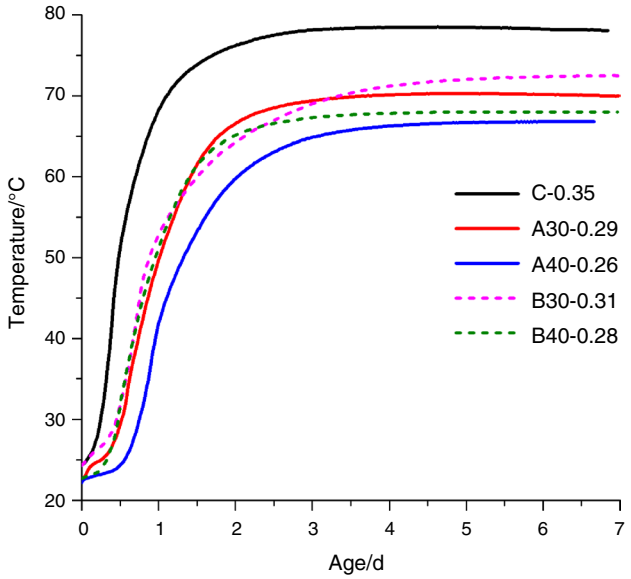

Fig. 5 The adiabatic temperature rise curves of concrete

Table 5 The adiabatic temperature rise of concrete mixes (°C)

Samples	Initial temperature	Equilibrium temperature	Adiabatic temperature rise	Reduction
C-0.35	24.3	78.1	53.8	–
A30-0.29	22.5	70.0	47.5	6.3
A40-0.26	22.2	66.8	44.6	9.2
B30-0.31	24.3	72.5	48.2	5.6
B40-0.28	22.7	68.0	45.3	8.5

0.35, the adiabatic temperature rise was 53.8 °C, while the concrete containing EFFSA or EFFSB experienced reduced adiabatic temperature rise. In addition, the adiabatic temperature rise was found to decrease with the increase in the EFFS content. These findings might be explained by the degree of cement hydration. The addition of EFFS reduced the cement content in the EFFS concrete system, which resulted in decreased hydration heat; moreover, the degree of hydration was also lower at a lower w/b ratio.

A comparison between the respective concrete samples containing the same contents of EFFSA and EFFSB reveals that the reduction of the adiabatic temperature rise decreased with the increased fineness of EFFS, which enhanced the pozzolanic activity of EFFSB. Moreover, the w/b ratio of the concrete mixed with EFFSB was higher than that of the concrete mixed with EFFSA. Therefore, the EFFSB concrete exhibited a higher adiabatic temperature rise. In other words, the increase in the fineness of EFFS is not conducive to reducing the adiabatic temperature rise of concrete.

Autogenous shrinkage

Based on the preceding results of the adiabatic temperature rise, the EFFSA concrete groups were selected for an autogenous shrinkage experiment. Figure 6 presents the autogenous shrinkage curves of the C-0.35, A30-0.29, and A40-0.26 concrete specimens within 7 d. As shown in the figure, the concrete containing EFFSA experienced reduced autogenous shrinkage. When the EFFSA replacement ratio was increased from 30 to 40%, the autogenous shrinkage decreased. This was expected, as EFFSA decelerated the hydration of the composite system, and the increase in the EFFSA content in the mixture led to declinations of the reaction rate and hydration degree of the concrete.

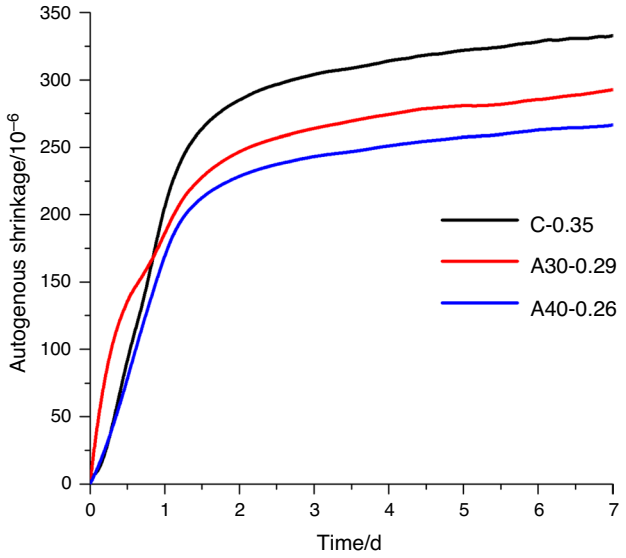

Fig. 6 Autogenous shrinkage of concretes

However, the autogenous shrinkages of the EFFS concretes were higher than that of plain cement concrete during the initial stage (within 1 day). As shown in Fig. 6, the autogenous shrinkages of A30-0.29 and A40-0.26 were higher than that of C-0.35 during the initial 20 h and 6.5 h, respectively. This may be attributed to the lower w/b ratio of the concrete containing EFFSA. A previous study [39] reported that, with the decrease in the w/b ratio, the internal relative humidity (RH) of concrete decreased, which can increase the early age shrinkage in concrete. In addition, the deformations caused by changes in temperature and humidity are large at an early age [40], which may increase the autogenous shrinkage. It is noteworthy that the increase in the EFFSA content in the mixture can improve the early age autogenous shrinkage. Moreover, the late-stage (after 1 day) autogenous shrinkages of the EFFSA concretes were found to be much lower than that of plain cement concrete with a higher w/b ratio (0.35). This is because EFFSA reduced the hydration degree in the compound system, which is the determining factor for the evolution of autogenous shrinkage.

Pore structure analysis

The pore size distributions of the hardened pastes at 28 d are presented in Fig. 7. Figure 7a reveals that the total porosities of the samples containing EFFS did not exhibit substantial differences from that of the plain cement sample, and samples containing EFFSB exhibited slightly higher total porosities. Under the condition of an equal w/b ratio (as shown in Fig. 3), the addition of EFFS had a negative effect on the degree of reaction, which resulted

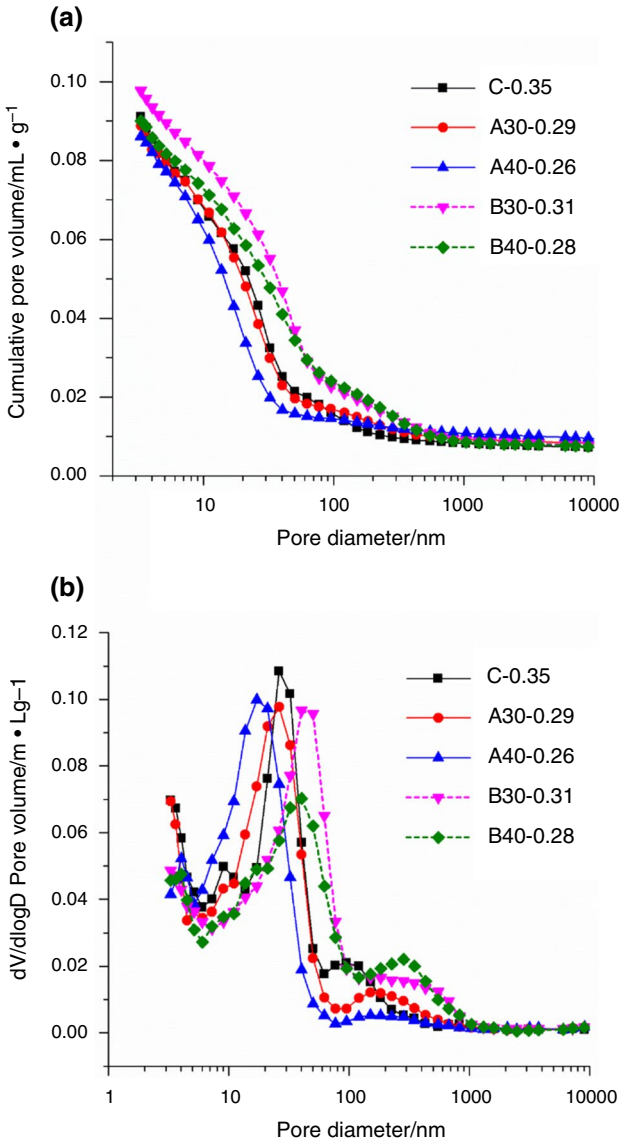

Fig. 7 Pore structure of hardened paste at 28 days. **a** Cumulative pore volumes; **b** pore size distributions

in the increase in the total porosity. However, the reduction of the w/b ratio can also improve the pore structure. It should be noted that the total porosity of sample C-0.35 was almost identical to that of sample A30-0.29, and the total porosity of the sample with a 40% proportion of EFFSA at a lower w/b ratio of 0.26 was notably decreased. Regarding the pore size distributions exhibited in Fig. 7b, the mixture samples presented curved profiles with main peaks between 10 and 50 nm. The samples containing EFFSB at a low w/b ratio had a slight increase in harmful pores (50–200 nm) as compared with the plain cement sample, whereas there were fewer harmful pores in the EFFSA samples at a lower w/b ratio. These results indicate that the reduction of the w/b ratio reduced the number of

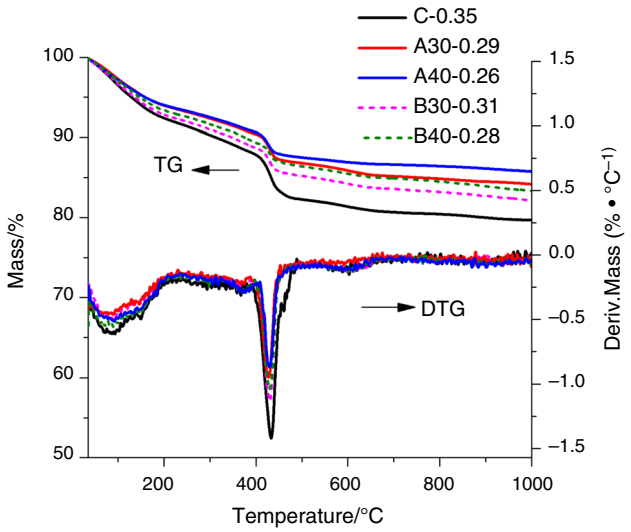

Fig. 8 TG-DTG curves of the hardened pastes at 28 d

harmful pores of the samples containing EFFS, and then refined the pore structures.

Thermogravimetric analysis

Figure 8 exhibits the TG-DTG curves of the hardened pastes at 28 d, which reveals that there was little difference between the main endothermic peak positions of the five groups; each DTG curve displays an endothermic peak at approximately 400–500 °C, a result associated with the CH dehydration. The CH characteristic peaks of the samples containing EFFS were significantly lower than that of the C-0.35 specimen. This is because the addition of EFFS reduced the cement content in the EFFS-cement systems, which resulted in decreased CH production. As determined by the TG-DTG results, the CH values calculated for the hardened pastes C-0.35, A30-0.29, A40-0.26, B30-0.31, and B40-0.28 were, respectively, 22.11%, 14.75%, 12.86%, 14.27%, and 12.14%. The samples containing the same content of EFFSA or EFFSB had similar CH contents. For the specimens with 30% and 40% replacement of cement by EFFSA and EFFSB, the CH contents were, respectively, 66.7%, 58.2%, 64.5%, and 54.9% that of the plain cement group, and were slightly lower than their respective cement content percentages. It is the comprehensive reflection of the following reasons: (i) the decrease in the amount of cement; (ii) the decrease in the w/b ratio of samples containing EFFS; (iii) the dilution and nucleation effects of EFFS; (iv) the pozzolanic activity of the EFFS which consumed part of the CH that was produced by cement hydration. Due to the relatively lower contents of Al_2O_3 and CaO in EFFS as compared to cement, EFFS has much lower pozzolanic activity [41]. Therefore, the CH required during the hydration process of the EFFS samples was primarily produced by cement hydration, which can improve the interfacial transition zone (ITZ).

Mechanical properties and chloride permeability of concrete

The effects of EFFS on the compressive strengths and splitting tensile strengths of the specimens are shown in Figs. 9a and b. The 28-day average compressive strength of the five groups of concrete specimens was 68 MPa. The compressive strengths of concrete containing EFFS were lower than that of the plain cement concrete at the early

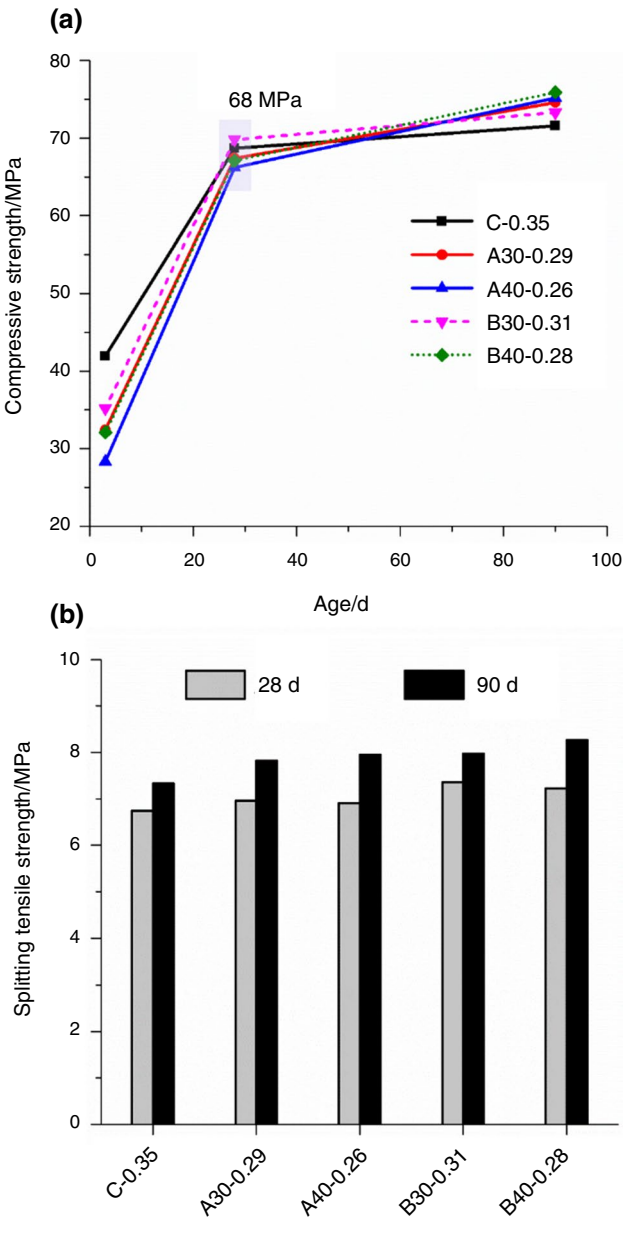

Fig. 9 **a** The compressive strength and **b** splitting tensile strength of concrete

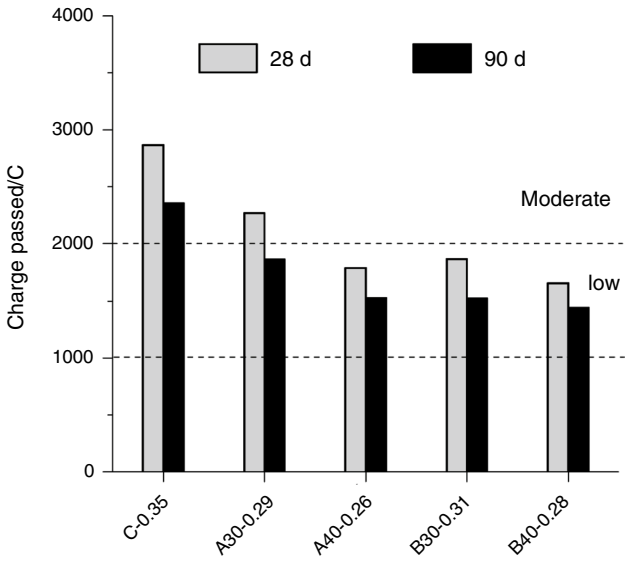

Fig. 10 The chloride ion permeability of concrete

age of 3 d. This is because the concrete samples with EFFS exhibited a slower rate of hydration than the control samples (as shown in Fig. 3). Thus, the compressive strength development was slower in the EFFS concrete than in the conventional cement concrete. The increase in the EFFSA or EFFSB replacement ratio from 30 to 40% was therefore not conducive to the development of the early age compressive strength. Nevertheless, increasing the fineness of EFFS can slightly increase the early age compressive strength. The particle size of EFFSB was smaller than that of EFFSA, and EFFSB therefore had a higher reaction speed at an early age (as shown in Fig. 3). The compressive strengths of all samples continued to increase with the extension of the curing period, and the later-age compressive strengths of the concrete specimens containing EFFS surpassed that of the plain cement concrete. This indicates that the reaction degree of EFFS increased with the age, and the contribution of EFFS to the compressive strength was also increased.

As shown in Fig. 9b, the splitting tensile strengths of the five groups of concrete were similar at the same age, but the concrete samples containing EFFS had slightly higher splitting tensile strengths than the plain cement concrete. On one hand, the concrete groups containing EFFS had lower w/b ratios, and lower free-water contents were therefore involved in the systems, which reduced the capillary porosity inside the concrete. On the other hand, the high content of amorphous silica (45.26%) present in EFFS reacted at the later ages, formed a secondary calcium silicate hydrate (C-S-H) gel, and improved the microstructure of the ITZ of the concrete [42, 43]. Therefore, the addition of EFFS improved the splitting tensile strength of the concrete.

The charge passed and chloride ion permeability of the C-0.35, A30-0.29, A40-0.26, B30-0.31, and B40-0.28 concrete specimens at 28 and 90 d are shown in Fig. 10. The charge passed of the concrete containing EFFS was decreased as compared with that of the plain cement concrete at the ages of 28 and 90 d. The results indicate that the pozzolanic reaction of EFFS improved the microstructure of the ITZ, and the lower w/b ratio reduced the connected pores, which was beneficial to the improvement of the chloride ion permeability. The chloride permeability grades of the EFFS concretes at 90 d were low. These results indicate that the incorporation of EFFS in concrete resulted in an improved chloride resistance property as compared to that of plain cement concrete.

Conclusions

1. The pastes mixed with 30% EFFSA and EFFSB exhibited lower yield stress and plastic viscosity as compared with the pure cement group. These results indicate that the workability of fresh pastes containing EFFS was improved. However, increasing the fineness of EFFS was found to decrease the workability of the EFFS-cement paste.
2. The replacement of cement with EFFS was found to decelerate the hydration heat of the binder. Within 72 h, the total heat emission of the samples containing EFFSB was higher than that of the samples containing EFFSA. This is because the finer particles may have acted as centers of nucleation and accelerated the cement hydration. Furthermore, the EFFSB reactivity was stimulated by the high temperature.
3. Under the same 28-day compressive strength level (68 MPa), the concrete containing EFFS exhibited a reduced adiabatic temperature rise. However, increasing the fineness of EFFS was not conducive to reducing the adiabatic temperature rise of concrete.
4. The concrete containing EFFS was found to have reduced late-stage (after 1 day) autogenous shrinkage. However, the autogenous shrinkages of the EFFS concretes were higher than that of plain cement concrete during the initial stage (within 1 day). It is notable that the increase in the EFFS content in the mixture can improve the early age autogenous shrinkage.
5. The MIP results revealed that a lower w/b ratio reduced the number of harmful pores in the samples containing EFFS, and then refined the pore structure of the mixed pastes. Due to the relatively lower concentration of CaO in EFFS than in cement, EFFS has a much lower pozzolanic activity than cement. The TG test results indicate that the pozzolanic reactions of EFFS consumed part of the CH, thereby improving the ITZ.

6. Although the addition of EFFS to concrete was harmful to the development of the early age compressive strength, it resulted in an increase in the later-age compressive and splitting tensile strengths of the concrete. The incorporation of EFFS in concrete was also found to result in a better chloride resistance property than that of plain cement concrete.

References

1. Wang Q, Huang Z, Wang D. Influence of high-volume electric furnace nickel slag and phosphorous slag on the properties of massive concrete. J Therm Anal Calorim. 2018;131:873–85.
2. Maria K. Early age properties of high-strength/high-performance concrete. Cem Concr Compos. 2002;24:253–61.
3. Zreiki J, Bouchelaghem F, Chaouche M. Early-age behaviour of concrete in massive structures, experimentation and modelling. Nucl Eng and Des. 2010;240:2643–54.
4. Zhang J, Hou D, Han Y. Micromechanical modeling on autogenous and drying shrinkages of concrete. Constr Build Mater. 2012;29:230–40.
5. Xie T, Fang C, Mohamad Ali MS, et al. Characterizations of autogenous and drying shrinkage of ultra-high performance concrete (UHPC): an experimental study. Cem Concr Compos. 2018;91:156–73.
6. Koo KM, Lee EB, Nam JS, et al. Analysis of hydration heat and autogenous shrinkage of high-strength mass concrete. Mag Concr Res. 2011;63:377–89.
7. Soliman AM, Nehdi ML. Effect of drying conditions on autogenous shrinkage in ultra-high performance concrete at early-age. Mater and Struct. 2011;44:879–99.
8. Nili M, Salehi AM. Assessing the effectiveness of pozzolans in massive high-strength concrete. Constr Build Mater. 2010;24:2108–16.
9. Simos N, Fallier M, Joos T, et al. Thermally induced cracking on the massive concrete structure of the NSLS II synchrotron and its engineering remediation. Eng Struct. 2020;212:110519.
10. Wang Q, Yan P, Feng J. Design of high-volume fly ash concrete for a massive foundation slab. Mag Concr Res. 2013;65:71–81.
11. Saha AK, Khan MNN, Sarker PK. Value added utilization of by-product electric furnace ferronickel slag as construction materials: a review. Resour Conserv Recy. 2018;134:10–24.
12. Choi YC, Choi S. Alkali-silica reactivity of cementitious materials using ferro-nickel slag fine aggregates produced in different cooling conditions. Constr Build Mater. 2015;99:279–87.
13. Komnitsas K, Zaharaki D, Perdikatsis V. Effect of synthesis parameters on the compressive strength of low-calcium ferronickel slag inorganic polymers. J Hazard Mater. 2009;161:760–8.
14. Li B, Huo B, Cao R, et al. Sulfate resistance of steam cured ferronickel slag blended cement mortar. Cem Concr Compos. 2019;96:204–11.
15. Komnitsas K, Zaharaki D, Perdikatsis V. Geopolymerisation of low calcium ferronickel slags. J Mater Sci. 2007;42:3073–82.
16. Peng Z, Tang H, Augustine R, et al. From ferronickel slag to value-added refractory materials: a microwave sintering strategy. Resour Conserv Recy. 2019;149:521–31.
17. Zhang Q, Ji T, Yang Z, et al. Influence of different activators on microstructure and strength of alkali-activated nickel slag cementitious materials. Constr Build Mater. 2020;235:117449.
18. Saha AK, Sarker PK. Expansion due to alkali-silica reaction of ferronickel slag fine aggregate in OPC and blended cement mortars. Constr Build Mater. 2016;123:135–42.
19. Liu X, Li T, Tian W, et al. Study on the durability of concrete with FNS fine aggregate. J Hazard Mater. 2019;381:120936.
20. Wang Z, Ni W, Jia Y, et al. Crystallization behavior of glass ceramics prepared from the mixture of nickel slag, blast furnace slag and quartz sand. J Non-Cryst Solids. 2010;356:1554–8.
21. Wang D, Wang Q, Xue J. Reuse of hazardous electrolytic manganese residue: detailed leaching characterization and novel application as a cementitious material. Resour Conserv Recy. 2020;154:104645.
22. Saha AK, Sarker PK. Sustainable use of ferronickel slag fine aggregate and fly ash in structural concrete: mechanical properties and leaching study. J Clean Prod. 2017;162:438–48.
23. Wang D, Wang Q, Zhuang S, et al. Evaluation of alkali-activated blast furnace ferronickel slag as a cementitious material: reaction mechanism, engineering properties and leaching behaviors. Constr Build Mater. 2018;188:860–73.
24. Wu Q, Wu Y, Tong W, et al. Utilization of nickel slag as raw material in the production of Portland cement for road construction. Constr Build Mater. 2018;193:426–34.
25. Sun J, Wang Z, Chen Z. Hydration mechanism of composite binders containing blast furnace ferronickel slag at different curing temperatures. J Therm Anal Calorim. 2018;131:2291–301.
26. Chen Y, Ji T, Yang Z, et al. Sustainable use of ferronickel slag in cementitious composites and the effect on chloride penetration resistance. Constr Build Mater. 2020;240:117969.
27. Gu YC, Li JL, Peng JK, et al. Immobilization of hazardous ferronickel slag treated using ternary limestone calcined clay cement. Constr Build Mater. 2020;250:118837.
28. Rahman MA, Sarker PK, Shaikh FUA, et al. Soundness and compressive strength of Portland cement blended with ground granulated ferronickel slag. Constr Build Mater. 2017;140:194–202.
29. Huang Y, Wang Q, Shi M. Characteristics and reactivity of ferronickel slag powder. Constr Build Mater. 2017;156:773–89.
30. Kim H, Lee CH, Ann KY. Feasibility of ferronickel slag powder for cementitious binder in concrete mix. Constr Build Mater. 2019;207:693–705.
31. Saha AK, Sarker PK. Effect of sulphate exposure on mortar consisting of ferronickel slag aggregate and supplementary cementitious materials. J Build Eng. 2019;28:101012.
32. Yang T, Yao X, Zhang Z. Geopolymer prepared with high-magnesium nickel slag: characterization of properties and microstructure. Constr Build Mater. 2014;59:188–94.
33. Yang T, Wu Q, Zhu H, et al. Geopolymer with improved thermal stability by incorporating high-magnesium nickel slag. Constr Build Mater. 2017;155:475–84.
34. Zhang Z, Zhu Y, Yang T, et al. Conversion of local industrial wastes into greener cement through geopolymer technology: a case study of high-magnesium nickel slag. J Clean Prod. 2017;141:463–71.
35. Cao R, Li B, You N, et al. Properties of alkali-activated ground granulated blast furnace slag blended with ferronickel slag. Constr Build Mater. 2018;192:123–32.
36. Mo L, Deng M, Tang M, Al-Tabbaa A. MgO expansive cement and concrete in China: past, present and future. Cem Concr Res. 2014;57:1–2.
37. Yin WS, Li XP, Sun T, Wang JP, Chen YZ, Yan G. Experimental investigation on the mechanical and rheological properties of high-performance concrete (HPC) incorporating sinking bead. Constr Build Mater. 2020;243:118293.
38. Luo T, Wang Q, Zhuang SY. Effect of ultra-fine ground granulated blast-furnace slag on initial setting time, fluidity and rheological properties of cement pastes. Powder Technol. 2019;345:54–63.

39. Wu LM, Farzadnia N, Shi CJ, Zhang ZH, Wang H. Autogenous shrinkage of high performance concrete: a review. Constr Build Mater. 2017;149:62–75.
40. Zhao HT, Jiang KD, Yang R, Tang YM, Liu JP. Experimental and theoretical analysis on coupled effect of hydration, temperature and humidity in early-age cement-based materials. Int J Heat Mass Tran. 2020;146:118784.
41. Yang T, Zhang ZH, Wang Q, Wu QS. ASR potential of nickel slag fine aggregate in blast furnace slag-fly ash geopolymer and Portland cement mortars. Constr Build Mater. 2020;262:119990.
42. Wang Q, Feng JJ, Yan PY. An explanation for the negative effect of elevated temperature at early ages on the late-age strength of concrete. J Mater Sci. 2011;46(22):7279–88.
43. Wang D, Wang Q, Huang Z. New insights into the early reaction of NaOH-activated slag in the presence of CaSO4. Compos Part B Eng. 2020;198:108207.